environmental microbiology

Environmental Microbiology (2015) **17**(6), 1926–1940 doi:10.1111/1462-2920.12465

Fate of arsenate following arsenite oxidation in *Agrobacterium tumefaciens* GW4

Qian Wang,[1] Dong Qin,[1] Shengzhe Zhang,[1] Lu Wang,[1] Jingxin Li,[1] Christopher Rensing,[2] Timothy R. McDermott[3] and Gejiao Wang[1]***

[1]*State Key Laboratory of Agricultural Microbiology, College of Life Science and Technology, Huazhong Agricultural University, Wuhan 430070, China.*

[2]*Department of Plant and Environmental Sciences, University of Copenhagen, Frederiksberg, Denmark.*

[3]*Department of Land Resources and Environmental Sciences, Montana State University, Bozeman, MT 59717, USA.*

Summary

The fate of arsenate (As^V) generated by microbial arsenite (As^{III}) oxidation is poorly understood. *Agrobacterium tumefaciens* wild-type strain (GW4) was studied to determine how the cell copes with As^V generated in batch culture. GW4 grown heterotrophically with mannitol used As^{III} as a supplemental energy supply as reflected by enhanced growth and increased cellular levels of NADH and ATP. Under low phosphate (Pi) conditions and presence of As^{III} oxidation, up to ~50% of the resulting As^V was taken up and found associated with the periplasm, membrane or cytoplasm fractions of the cells. Arsenic was found associated with proteins and polar lipids, but not in nucleic acids or sugars. Thin-layer chromatography and gas chromatography–mass spectrometry analysis suggested the presence of arsenolipids in membranes, presumably as part of the bilayer structure of the cell membrane and replacing Pi under Pi-limiting conditions. The potential role of a Pi-binding protein (PstS) for As^V uptake was assessed with the His-tag purified protein. Intrinsic tryptophan fluorescence spectra analysis suggests that PstS can bind As^V, but with lower affinity as compared with Pi. In early stationary phase cells, the As^V : Pi ratio was approximately 4.3 and accompanied by an altered cell ultrastructure.

Received 23 December, 2013; accepted 20 March, 2014. For correspondence. *E-mail gejiao@mail.hzau.edu.cn; Tel. (+86) 27 87281261; Fax (+86) 27 87280670. **E-mail timmcder@montana.edu; Tel. (+1) 406 994 2190; Fax (+1) 406 994 3933.

Introduction

Arsenic (As) is the most common toxic element in the environment, ranking first on the U.S. Superfund List of Hazardous Substances and is responsible for mass poisoning throughout Asia (Chakraborti *et al.*, 2009; Rodríguez-Lado *et al.*, 2013). In the environment, transport, bioavailability and accumulation of As in biological endpoints is dependent on chemical speciation, with arsenite (As^{III}) and arsenate (As^V) being the primary arsenicals found in the environment. Microbial redox transformations are recognized as being important contributors to equilibrium levels of As^{III} and As^V (Cullen and Reimer, 1989; Inskeep *et al.*, 2001; Oremland and Stolz, 2005; Stolz *et al.*, 2006).

Microbial As^{III} oxidation and As^V reduction both serve as detoxification and/or energy-generating functions, depending on the organism (Stolz *et al.*, 2006; Páez-Espino *et al.*, 2009). Reasonable models exist for understanding how microorganisms deal with modest levels of arsenic in their environment (Slyemi and Bonnefoy, 2012); however, documentation of microbial resistance to millimolar concentrations of As^V or As^{III} has become common (e.g. Achour *et al.*, 2007; Fan *et al.*, 2008; Cai *et al.*, 2009). The basis for resistance to such high concentrations is actually still poorly understood, although it is assumed that As^V taken up by the cell is reduced to As^{III} by ArsC (part of the Ars-based As detoxification system). As^{III} is the substrate for the antiporters ArsB or Acr3, which removes it from the cell. As^{III} taken up via aquaglyceroporin (Liu *et al.*, 2004) or hexose permeases (Liu *et al.*, 2006) is likewise exported via ArsB or Acr3, the efflux function of which is assumed to occur at rates that exceed uptake and therefore avoid accumulation of the toxic metalloid. For microbes that reduce As^V via ArsC or by ArrAB (anaerobically respiring As^V), export of As^{III} is the limiting factor concerning arsenic resistance (Rosen, 2002). However, for As^{III}-oxidizing organisms, As^V accumulates in the medium (at least in the experimental setting), becoming substrate for phosphate (Pi) transporters that then actively take up As^V into the cell. What is the fate of this As^V and how does the cell accommodate such situations?

This question has taken on more importance given the recent discovery showing that genes essential for As^{III}

oxidation are derepressed under low-Pi conditions (Kang *et al*., 2012). High Pi levels in any environment are typically not the norm, as even in fertile soils soluble Pi levels do not exceed the low micromolar range (Larsen and Court, 1961). When combined with high As levels (e.g. geothermal- or mine-impacted locations), this becomes a cell survival issue for As^{III}-oxidizing microbes, where as a result of their redox activities the As : Pi ratios can potentially exceed the capacity of any Pi transport system to differentiate these analogues and thus lead to As^{V} uptake. This has been shown to occur with low-affinity, hig-velocity-type Pi transporters (Willsky and Malamy, 1980b; Hsieh and Wanner, 2010) or the high-affinity Pst system when the As^{V} : Pi ratio ≥ 10 (Willsky and Malamy, 1980b). Once in the cell, As^{V} can substitute for Pi in biochemical reactions; however, because of the instability of the arsenoester bonds, it fails to replace Pi in key structures such as nucleic acids or ATP. Still, biosynthesis of arsenosugars (Edmonds and Francesconi, 1987) and arsenolipids (Morita and Shibata, 1988) has been documented, and thus it is of interest to determine how and where these molecules are used in the cell.

We have been developing *Agrobacterium tumefaciens* strains GW4 and 5A as models for understanding the physiology and genetics of bacterial As^{III} oxidation. In a prior study, *A. tumefaciens* GW4 was isolated from As-contaminated aquifer sediments and shown to actively oxidize As^{III} (Fan *et al*., 2008). In this study, we examined the fate of As^{V} generated by GW4 via comparing the wild-type strain with a specific Δ*aioA* mutant that is devoid of As^{III}-oxidizing activity. GW4 was found to gain energy from As^{III} oxidation as indicated by enhanced growth relative to controls, and was confirmed by finding increased cellular NADH and ATP in As^{III}-oxidizing cells. When high As^{V} : Pi ratios developed under batch conditions, As^{III}-oxidizing cultures began accumulating As^{V} in the periplasm, membrane and cytoplasm. Membrane lipid structure and composition were altered; however, there was no evidence that the cells suffered growth defects.

Results

Genetic organization of the aio locus and aioA mutation

Draft genome sequencing of *A. tumefaciens* GW4 revealed that an arsenic island containing arsenite oxidase genes *aioXSRBA* and phosphate-related genes *phoB1* and *pstSCAB* (Supporting Information Table S3) is highly similar to that of *A. tumefaciens* strain 5A (Kang *et al*., 2012; Liu *et al*., 2012) (Supporting Information Fig. S1). The *aioXSRBA* genes are in the same order and orientation, and are located directly adjacent to *phoB1* and the *pstSCAB* operon (Supporting Information Fig. S1), referred to as *phoB-1* and *pstS-1*, *pstC-1*, *pstA-1* and *pstB-1* by Kang and colleagues (2012).

To investigate how the cell responds to the accumulation of As^{V} in its environment, an *aioA* deletion strain (Δ*aioA*) and the complemented mutant strain (Δ*aioA*-C) were constructed. The successful mutation and the complementation were confirmed by PCR using the primers PMaioA-1F/PMaioA-1R and PMaioA-2F/PMaioA-2R (Supporting Information Fig. S2), and by sequencing the amplicons. In verification tests, the Δ*aioA* mutant was found to be negative for As^{III} oxidation (see below). Strain Δ*aioA*-C, which carries the *aioBA* genes and upstream DNA *in trans* on plasmid pCPP30, was complemented back to wild-type status with regards to As^{III} oxidation.

Effects of As^{III}/As^{V} on growth of strain GW4

When well-washed cells were incubated in a minimal mannitol ammonium ($MMNH_4$) liquid media lacking added phosphate (Pi), none of the strains would grow, regardless of whether As^{III}/As^{V} was added (data not shown) and was interpreted as Pi being essential for growth. When provided As^{V} under low-Pi conditions (0.1 mM), final viable cell counts tended to be slightly higher with As^{V} than in the absence of added arsenic, although the differences were not significant at most time points (Fig. 1A–C). However, under low-Pi and normal-Pi conditions (1 mM), the addition of As^{III} resulted in significantly enhanced growth for the wild-type strain GW4 beyond that provided by the 54.8 mM mannitol in the medium (Fig. 1A and D), indicating As^{III} oxidation in this strain yields energy for growth. Consistent with this interpretation, the Δ*aioA* mutant failed to demonstrate increased growth as a function of As^{III} addition (Fig. 1B and E). Providing the *aioBA* genes *in trans* (strain Δ*aioA*-C) reversed the Δ*aioA* mutant null phenotype back to wild-type status with respect to growth response to added As^{III} (Fig. 1C and F). Further evidence of As^{III} being used as an energy source was obtained by examining NADH and ATP concentrations in the three different strains. At early-to-mid log phase cultures, cellular levels of NADH and ATP (Supporting Information Fig. S3) were both significantly increased in GW4 and Δ*aioA*-C cells provided with As^{III}, but not in the Δ*aioA* mutant, regardless of As^{III} treatment.

A Pi treatment effect on growth was discernible in cells where growth was not dependent or enhanced by As^{III} oxidation (Fig. 1A, D, C and F). With the addition of As^{III}, final viable cell counts for the As^{III}-oxidizing wild-type cultures were essentially the same regardless of the level of starting Pi (Fig. 1A and D). However, in the absence of As^{III} oxidation (i.e. heterotrophic growth only), cultures provided with additional Pi attained a higher final cell density (Fig. 1: compare panels A and D, B and E, C and F). Across the experiments, cell response to As^{III} in relation to Pi effects were internally consistent, final cell

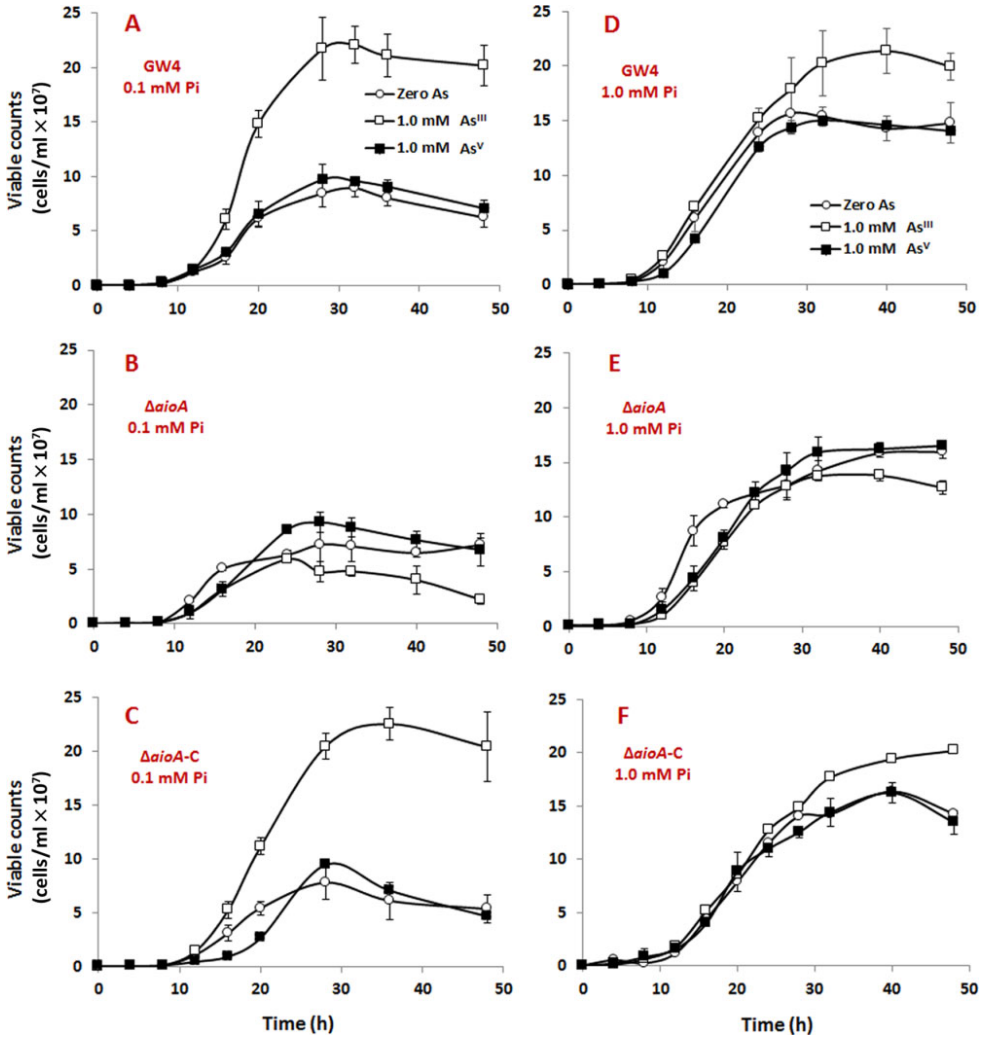

Fig. 1. Growth curves of *A. tumefaciens* strains GW4, Δ*aioA* and Δ*aioA*-C in the presence of zero added arsenic or as 1.0 mM As^{III} or 1.0 mM As^{V}:
A, B and C. Low Pi.
D, E and F. Normal Pi.
Data are shown as the mean of three replicates, with the error bars illustrating one standard deviation.

counts for the Δ*aioA* mutant were essentially the same as the wild type cultured in the absence of As^{III} (Fig. 1, compare panels A and D against B and E). Further, though not identical, the growth profile for the complemented mutant Δ*aioA*-C was highly similar to the parental wild-type strain and served to confirm the effect of As^{III} oxidation on the ability of GW4 to fully capitalize on the added Pi (compare Fig. 1, panels A and D with panels C and F).

The As^{III} oxidation profiles for each strain and Pi condition are shown in Fig. 2. Experimentally, this data is linked to all other data described herein, and for accounting purposes, we present all As^{III} and As^{V} data in terms of molar concentrations of arsenic on a culture-volume basis (Fig. 2). For the wild-type strain under low-Pi conditions, As^{V} accumulation in the culture media commenced within the first few hours of cultivation (Fig. 2A), whereas apparent As^{III} oxidation under normal-Pi conditions was phase-shifted several hours (Fig. 2D). Similar results were observed for strain Δ*aioA*-C, and as expected, there was no As^{V} accumulation in the Δ*aioA* culture fluids because of its inability to oxidize As^{III} (Fig. 2B and E). At early-to-mid log phase Pi-limited GW4 cells, the As^{V} formed began to accumulate in cell biomass as indicated by the decline in As^{V} in the culture fluids while As^{III} levels also decreased because of As^{III} oxidation (Fig. 2A). Cellular uptake of As^{V} was verified by directly measuring cell biomass arsenic contents (Table 1). When provided with normal Pi, the decline in As^{III} levels because of As^{III} oxidation tracked with the accumulation of As^{V} in the medium (Fig. 2D and F). Under such conditions, As^{III}-oxidizing cells did not accumulate the As^{V} they generated (see below). As

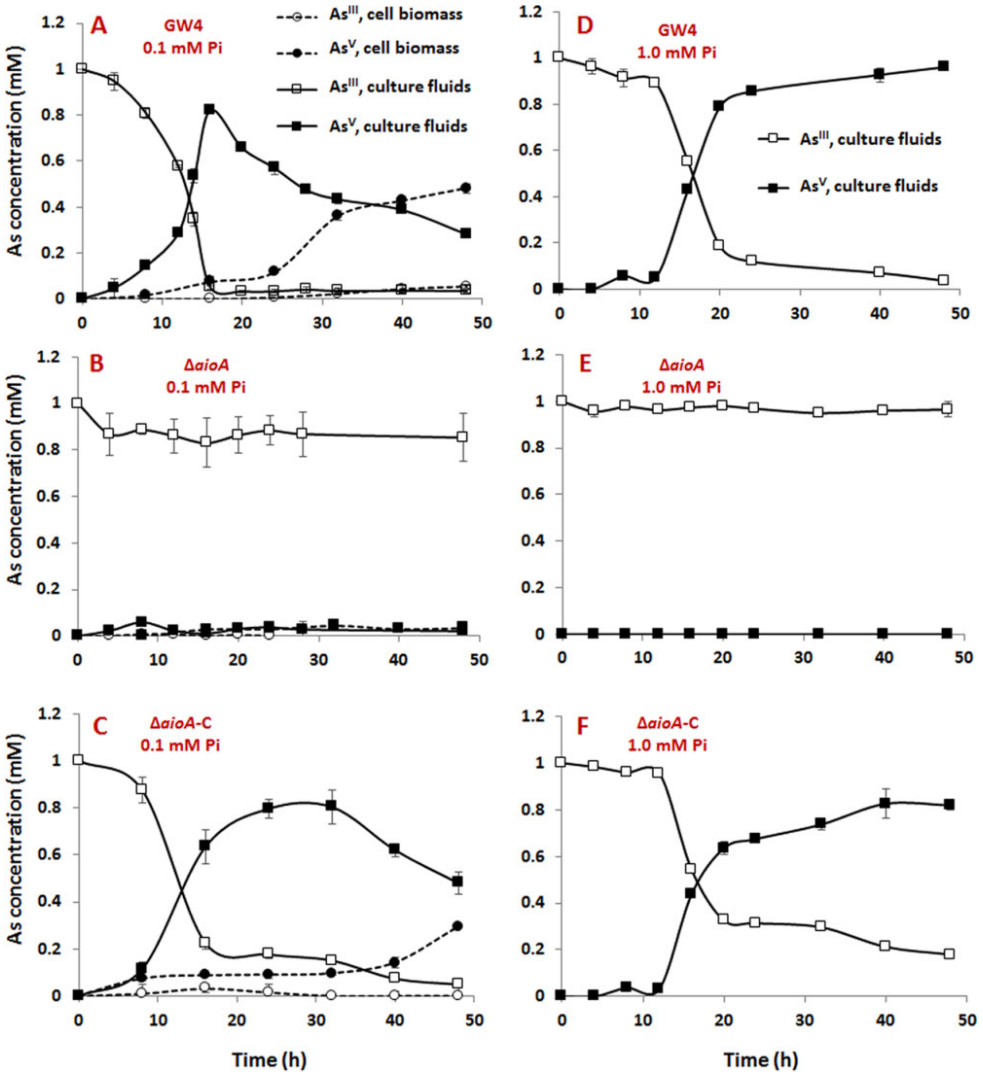

Fig. 2. As^III^ oxidation curves and distribution of arsenic in cultures and media. The amounts of As^III^ and As^V^ in culture fluids and cell biomass were calculated based on culture volume so as to maintain common units for accounting of total arsenic added. Data symbols shown in panel A are the same for panels B and C, and data symbols shown in panel D are the same for panels E and F. As^III^ and As^V^ concentrations in the cell biomass or cultural fluids were measured using HPLC-HG-AFS. Data are shown as the mean of three replicates, with the error bars illustrating one standard deviation.

expected, As^V^ levels in the Δ*aioA* culture fluids were quite low and are interpreted here as representing background levels of As^V^ present in the As^III^ reagent (Fig. 2B and E).

Pi levels were also tracked in the culture media (Fig. 3). In GW4 cells cultured under low-Pi conditions, the enhanced cell density in cultures gaining growth-promoting energy from As^III^ oxidation appeared to translate into increased Pi consumption relative to cells growing strictly heterotrophically (Fig. 3A). Under normal-Pi growth conditions, however, medium Pi depletion did not differ between As^III^ treatments (Fig. 3D–F), even though final cell numbers were ~ 25% greater in the

Table 1. As^V^ and Pi associated with washed cell biomass of GW4 cells oxidizing As^III^.

	Pi growth conditions	
	Low	Normal
Element	mmol g^{-1}	
As^V^	1.3 ± 0.16	0
As^III^	0.07 ± 0.001	0
Pi	0.3 ± 0.006	1.3 ± 0.14
Total	1.67 ± 0.017	1.3 ± 0.014

Biomass samples were taken after 32 h incubation (early stationary phase cells; see Fig. 1A).

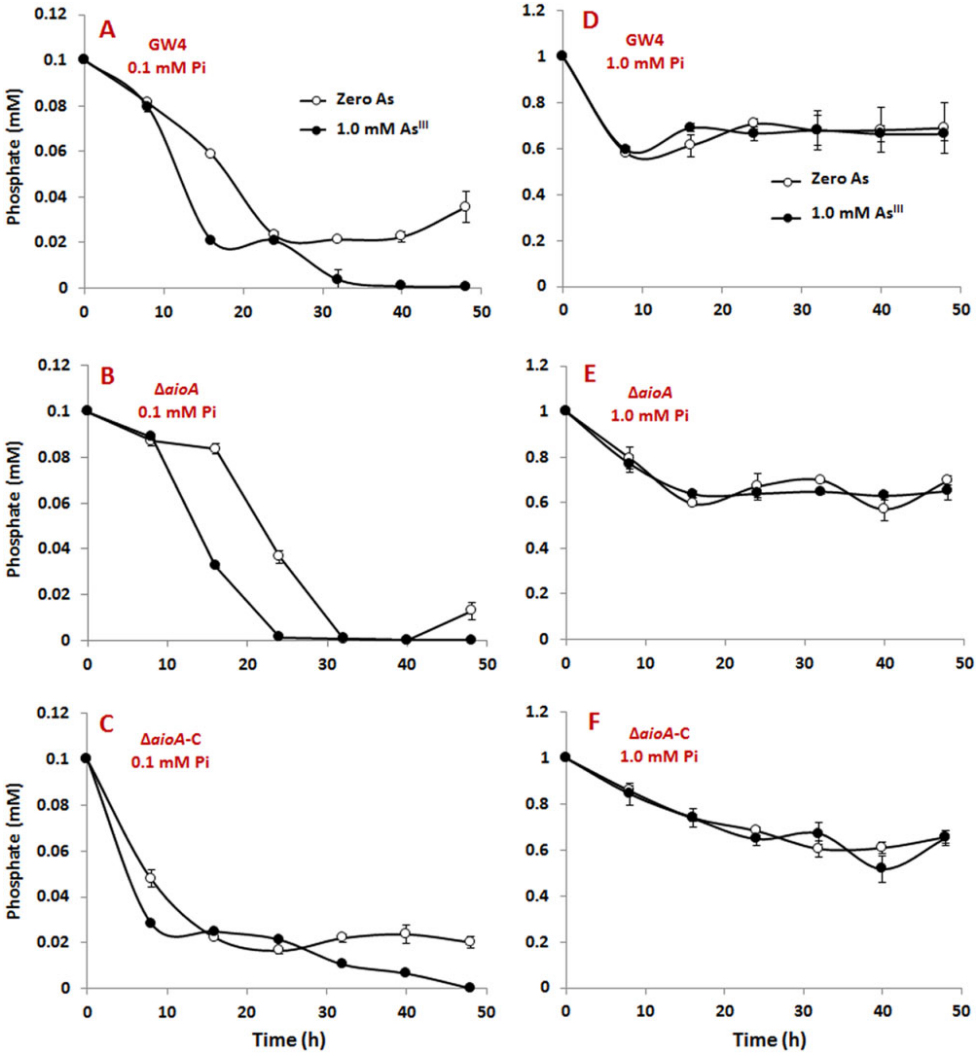

Fig. 3. Monitoring Pi concentrations in cell-free culture fluids of strains GW4, Δ*aioA* and Δ*aioA*-C:
A, B and C. Low Pi
D, E and F. Normal Pi.
Data symbols shown in panel A are the same for panels B and C, and data symbols shown in panel D are the same for panels E and F. Data are shown as the mean of three replicates, with the error bars (where visible) illustrating one standard deviation.

As^{III}-oxidizing cultures (refer to Fig. 1D and F). Final levels of Pi in the culture fluids of normal-Pi treatments were very similar (range: 0.57–0.71 mM; average: 0.68 mM, 0.65 mM and 0.63 mM Pi for GW4, Δ*aioA*, and Δ*aioA*-C respectively), regardless of As^{III} treatment, implying that the cellular Pi requirement had been satisfied.

Fate of As^V

In culture fluids of log phase As^{III}-oxidizing cultures (GW4 and Δ*aioA*-C), Pi was depleted to roughly 20 μM (16 h, Fig. 3) and As^V accumulated to where As^V:Pi ratios were roughly 40. This is a condition favouring As^V uptake, regardless of the type of transporter engaged and is indicated by decreasing levels of As^V in the culture fluids of these organisms (Fig. 2). To begin examining the fate of cellular As^V, cells were harvested at 32 h (early stationary phase), digested and assayed for As^{III} and As^V. Consistent with the data in Fig. 2, no arsenic was detected in whole cell preparations harvested from normal-Pi media, whereas Pi content was 1.3 mmol ± 0.14 per gram cell dry weight (g-dw^{-1}, Table 1). By contrast, GW4 from low-Pi media contained 1.3 mmol ± 0.16 As^V and 0.3 ± 0.006 mmol Pi g-dw^{-1} (Table 1), remarkably an As^V : Pi ratio of 4.3.

Subsequent analysis then sought to determine how the arsenic was distributed within the cells. In these experiments, only As^{III}-treated cells for all three strains were examined. On a per gram cell dry weight basis, relative distributions of As^V and As^{III} were quite similar in GW4 and

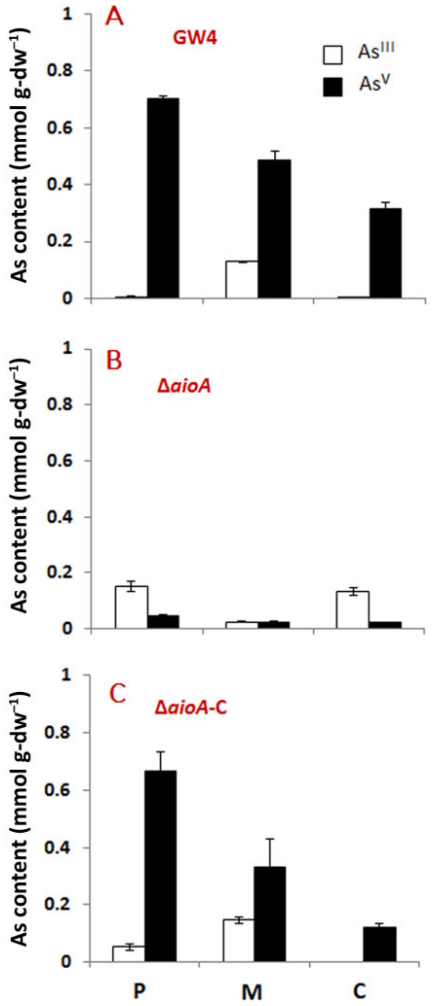

Fig. 4. Cellular distribution of arsenic:
A. GW4.
B. Δ*aioA*
C. Δ*aioA*-C.
Cells were harvested after 32 h incubation in low-Pi $MMNH_4$ medium with the addition of 1.0 mM As^{III}. Cell biomass was fractionated into periplasm (P), membrane (M) and cytoplasm (C). As^{III} and As^{V} contents were monitored using HPLC-HG-AFS. Data are shown as the mean of three replicates, with the error bars (where visible) illustrating one standard deviation.

Δ*aioA*-C (Fig. 4). Smaller amounts of As^{III} were detected in the membrane fractions of GW4 and Δ*aioA*-C, although appreciably greater than in the periplasm and cytoplasm (Fig. 4A and C). As expected, very little As^{V} could be detected in Δ*aioA* (presumed background), with As^{III} being the chief As species and primarily restricted to the periplasm and cytoplasm fractions (Fig. 4B). Further analysis then examined arsenic in extracted and digested proteins and nucleic acids. Similar to overall cellular distribution patterns (Fig. 4), GW4 and Δ*aioA*-C were again very similar in terms of relative levels of As^{III} and As^{V} in proteins, though very different from Δ*aioA* (Fig. 5). For the Δ*aioA* mutant, arsenic was primarily As^{III} (Fig. 5). For all strains, arsenic was not detected in DNA, RNA, nor as arsenosugars (data not shown).

As^{V} was detected and characterized in polar lipids. Thin-layer chromatography (TLC) illustrated that with the As^{III}-oxidizing strains GW4 and Δ*aioA*-C, the migration of higher molecular weight polar lipids was slightly retarded relative to those of cells where As^{V} was not present in significant amounts (Fig. 6A). There was no As-specific shift observed in the comparable lipid spots of Δ*aioA*, which could not produce As^{V} (Fig. 6A). High-performance-liquid-chromatography hydride generation atomic fluorescence spectrometry (HPLC-HG-AFS) was then used to quantify arsenic in these polar lipids. Strains GW4 and Δ*aioA*-C contained 0.4 ± 0.04 and 0.5 ± 0.10 mmol As^{V}g-dw^{-1} respectively, greatly exceeding the As^{V} in the polar lipids of strain Δ*aioA* (Fig. 6B).

The structures of the As^{V}-containing polar lipids were then explored with gas chromatography–mass spectrometry (GC-MS). In addition to the standard (21.6 min), there were five additional peaks detected in all three strains that exhibited identical elution times (Supporting Information Fig. S4). In the absence of As^{III}, the polar lipid profiles for all three strains were essentially identical (Supporting Information Fig. S4D–F). However, the relative abundance of these five lipids varied consistently as a function of As^{V} being available from As^{III} oxidation. Cis-9-hexadecenoic and Cis-10-hexadecenoic acids were both depleted in GW4 and Δ*aioA*-C, but unchanged, or relatively so, in the mutant (Fig. 7). In contrast, 2-octyl-cyclopropaneoctanoic acid was significantly increased in GW4 and Δ*aioA*-C (Fig. 7), whereas hexadecanoic acid and nonadecanoic acid content appeared unchanged in all three strains regardless of the arsenic treatment and As^{III} oxidation capacity. Each of these polar lipids have been documented in bacteria previously (Cox and

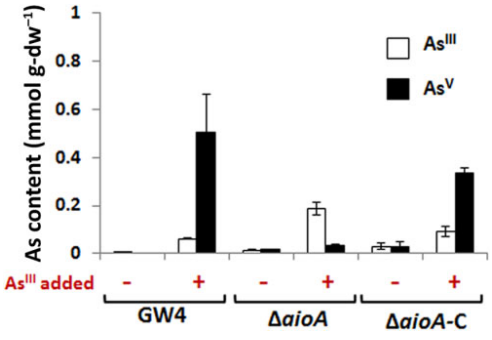

Fig. 5. As^{III} and As^{V} content in the total protein fraction of *A. tumefaciens* strains GW4, Δ*aioA* and Δ*aioA*-C after 32 h cultivation in low-Pi conditions with (+) or without (–) the addition of 1.0 mM As^{III}. As^{III} and As^{V} contents were monitored using HPLC-HG-AFS as described in Experimental Procedures. Data are shown as the mean of three replicates, with the error bar (where visible) illustrating one standard deviation.

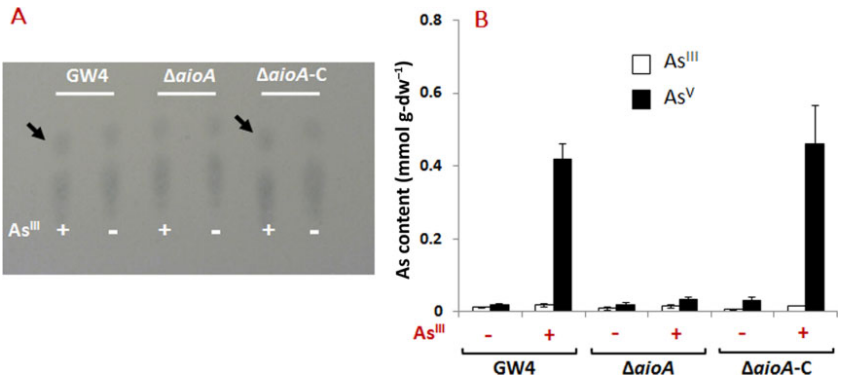

Fig. 6. Analysis of polar lipids in *A. tumefaciens* strains GW4, Δ*aioA* and Δ*aioA*-C.
A. The TLC profile of high molecular weight polar lipids. The lipid spots labelled by black arrows represent the polar lipids with altered molecular weight resulting from As^V incorporation into the lipid structure.
B. Arsenic contents of total cellular polar lipids.
Data are shown as the mean of three replicates, with the error bar (where visible) illustrating one standard deviation.

Wilkinson, 1989; Konova *et al*., 2005; Rakotomanga *et al*., 2005; Mayilraj *et al*., 2006; Dejoye *et al*., 2011).

Cell morphology

The effect of arsenic on bacterial morphology was examined using transmission electron microscopy (TEM). Under low-Pi conditions and with As^{III} addition (i.e. As^V-generating conditions), electron density of the cytoplasm was distinctly altered in As^{III}-exposed GW4 cells (Supporting Information Fig. S5). In addition, the cell cytoplasm contents appeared to pull away from the cell membrane structure (Supporting Information Fig. S5). In contrast, visually the cell ultrastructure and envelope of the Δ*aioA* mutant appeared largely unchanged (Supporting Information Fig. S5).

A

Relative peak area

Retention time (min)	Strain					
	GW4		ΔaioA		ΔaioA -C	
	+ As^{III}	- As^{III}	+ As^{III}	- As^{III}	+ As^{III}	- As^{III}
Standard (21.6)	100%	100%	100%	100%	100%	100%
16.7	3.3%	14.8%	17.1%	17.0%	3.4%	18.4%
17.3	20.9%	20.5%	22.2%	20.7%	21.0%	26.2%
19.2	1.5%	9.7%	10.8%	6.0%	0.6%	8.0%
23.7	21.4%	4.1%	4.7%	7.7%	16.0%	6.9%
24.1	48.2%	49.7%	45.3%	50.1%	44.9%	47.1%

B

Retention time (min)	Molecular structure formula	Name
16.7		Cis-9-Hexadecenoic acid
17.3		Hexadecanoic acid
19.2		Cis-10-Heptadecenoic acid
23.7		2-octyl-cyclopropaneoctanoic acid
24.1		Nonadecanoic acid

Fig. 7. Characterization of polar lipids in *A. tumefaciens* GW4, Δ*aioA* and Δ*aioA*-C cultured in the presence or absence of As^{III}.
A. Abundance of each relative to an internal standard (as depicted in Supporting Information Fig. S4).
B. Predicted tail structures for the lipids at each retention time.

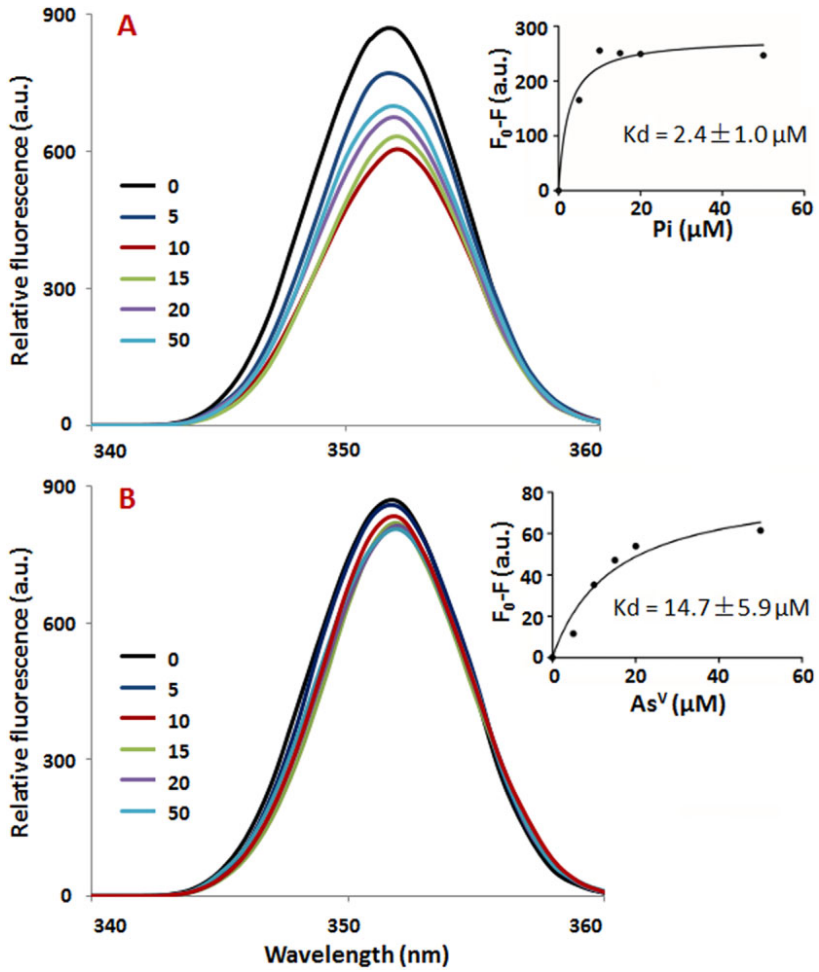

Fig. 8. Interaction of PstS with Pi and As^V as measured by relative intrinsic fluorescence. Purified PstS (0.6 μM) was incubated with Pi or As^V (0, 5, 10, 15, 20 or 50 mM).
A. Fluorescence quenching observed when PstS was incubated with incremental increases of Pi.
B. Fluorescence quenching observed when PstS was incubated with incremental increases of As^V (10–50 mM AsV). Fluorescence changes at 352 nm were analysed by GraphPad Prism 5 and used to calculate Kd values.

Functional analysis of PstS

In order to more closely examine the ability of GW4 to take up As^V, we studied PstS1. In other bacteria, the *pstS* gene (Supporting Information Fig. S1) has been shown to encode a periplasmic Pi-binding protein (Medveczky and Rosenberg, 1970) involved with Pi transport via the high affinity PstCAB system (Willsky and Malamy, 1980a). Consequently, we first assessed whether *pstS1* is subject to As^{III}-based regulation. Based on SDS-PAGE analysis and mass spectrometry of a dominant protein band, the PstS1 protein in GW4 was found to be increased in As^{III}-exposed cells (Supporting Information Fig. S6A) and is consistent with the *pstS1*::*lacZ* expression activity recently reported by Kang and colleagues (2012) with *A. tumefaciens* strain 5A. The *pstS1* gene was then PCR-cloned, over-expressed and His_6-tag purified (Supporting Information Fig. S6B), and then employed in assays to examine its affinity for Pi, As^V or As^{III} (Fig. 8). The three tryptophan residues (W_{133}, W_{145} and W_{156}) made this protein a good candidate for tryptophan-based intrinsic fluorescence assays. In binding assays containing incremental increases of Pi, As^{III} or As^V, fluorescence quenching of PstS1 was consistent with PstS1 not binding As^{III} (no fluorescence quenching, results not shown), but capable of binding both Pi (Fig. 8A) and As^V with different affinities (Fig. 8B). As estimated from calculated Kd values, PstS1 demonstrated an approximate sixfold greater affinity for Pi relative to As^V (Fig. 8).

Discussion

The general aim of this study was to track the physiologic features of GW4 during As^{III} oxidation, to examine the cellular fate of the As^V it generates (i.e. microbial As^{III} oxidation) and to assess the interactive effect of Pi. We obtained convincing evidence of GW4 being capable of acquiring growth-promoting energy from As^{III} oxidation as opposed to oxidizing As^{III} for detoxification purposes. This conclusion is supported by analyses that showed significantly enhanced growth when provided As^{III} (Fig. 1), correlating with enhanced cellular NADH and ATP (Supporting Information Fig. S3). This was not the case for the Δ*aioA* mutant, and while the complemented mutant Δ*aioA*-C carrying the *aioBA* genes *in trans* did not always perfectly match GW4, its responses were similar enough

to GW4 in all features examined to satisfactorily demonstrate that the growth phenotype and metabolite profile of the Δ*aioA* mutant was in large part directly because of the lack of As^{III} oxidation capacity. When viewed as a whole, the data provides clear evidence of As^{III} chemolithotrophy-based, enhanced heterotrophic growth and as such is similar to that reported for *Hydrogenophaga* (vanden Hoven and Santini, 2004). Finding elevated ATP in the As^{III}-oxidizing strains but not the Δ*aioA* mutant (Supporting Information Fig. S3) was not surprising. However, significantly enhanced NADH levels (Supporting Information Fig. S3) were unexpected given the current model of electron transport associated with As^{III} oxidation, which suggests the As^{III} oxidase enzyme directly transfers electrons to a c-type cytochrome (vanden Hoven and Santini, 2004; Santini *et al*., 2007; Lieutaud *et al*., 2010; van Lis *et al*., 2013). If the increased NADH in GW4 derived directly from As^{III} oxidation, this would suggest that electron transport involving As^{III} oxidase in this organism involves additional step(s) prior to passing electrons to a c-type cytochrome.

Because the carbon source and amount were fixed in all treatments, growth differences were linked to the different Pi and As^{III} treatments, and to strain *aioA* genotype. In assessing the fate of As^{V}, the higher Pi level was selected in order to hold the cells in a state of luxurious Pi for comparative purposes, while the low-Pi level was chosen so as to intentionally manipulate As^{V} : Pi ratios in batch culture in a time-convenient fashion to facilitate ordered observations of cellular behaviour as the culture medium Pi levels were depleted. Energy and growth yield gains from As^{III} oxidation was apparent under both Pi conditions (Fig. 1, Supporting Information Fig. S3), but Pi availability exerted obvious effects as the apparent energy boost from As^{III} oxidation was relatively greater in low-Pi conditions as compared with normal-Pi conditions (e.g. compare Fig. 1A–D). This differential Pi effect suggests that Pi-limited GW4 cells were somehow more efficient in maximizing the energy benefit from As^{III} oxidation. Greater growth was also observed with the Δ*aioA* mutant under normal-Pi conditions (compare Fig. 1B and E), indicating the low-Pi treatment was indeed a limiting condition, independent of, and in addition to, energy gained from As^{III} oxidation.

The As^{III} oxidation profiles observed for the different Pi conditions were interesting from the standpoint of Pi-related *aio* gene regulation. Under low-Pi conditions, GW4 As^{III} oxidation was apparent at the first sampling time (4 h, Fig. 2A), during which time Pi levels in the medium were between 80–100 μM (Fig. 3). Under normal-Pi culturing conditions (starting Pi = 1.0 mM), As^{III} oxidation was apparent (Fig. 1D) when the medium Pi concentration was roughly 700 μM (Fig. 3). Thus in both cases, As^{III} oxidation was detectable when Pi levels were much higher than what might be predicted based on the experiments reported by Kang and colleagues (2012). In the latter study, induction of the *aioBA* genes in *A. tumefaciens* strain 5A was shown: (i) to not occur until Pi levels decreased to < 10 μM; (ii) to coincide with the induction of alkaline phosphatase (the indigenous bacterial Pi stress reporter enzyme); and (iii) to be somehow influenced by PhoB1/PhoB2. Furthermore, induction of *pstS1* and *phoB1* in strain 5A (see gene arrangements in Supporting Information Fig. S1) were under the control of both PhoB and ArsR-1 (Kang *et al*., 2012), partially explaining how the regulatory influences of As^{III} and Pi are integrated. Integration of the *aio* and *pst/pho* regulatory circuitries is not restricted to *A. tumefaciens*, however, as this was also inferred by microarray studies of *Herminiimonas arsenicoxydans* that illustrated up-regulation of *pst* and *pho* genes in the same approximate time frame of *aio* genes being transcribed (Cleiss-Arnold *et al*., 2010). Clearly, more effort will be required to generate conceptual models that more fully explain how the Pst/Pho and Aio systems work together in different organisms.

In the wild-type GW4 cultured in low Pi, As^{V} uptake became apparent at mid-log phase (Fig. 2), corresponding to when As^{V} levels had accumulated to roughly 800 μM (Fig. 2A), and Pi levels had been depleted to approximately 20 μM (Fig. 3A). As such, this created an environment wherein the As^{V} : Pi ratio was ~ 40, a scenario where As^{V} uptake could be facilitated by even phosphate specific transporters such as the PstSCAB system (Willsky and Malamy, 1980a,b). In this regard, the *pstSCABphoU* operon located adjacent to the *aioXSRBAcytC*$_{552}$ locus (Supporting Information Fig. S1) was of special interest to our labs. A recent survey of genomes of As^{III}-oxidizing microorganisms (Li *et al*., 2013) described partial or whole *pst-pho* and *phn* operons located adjacent to gene clusters involved in arsenic metabolism [*ars*, *aio*, *acr3*, etc.; referred to as arsenic islands (Silver and Phung, 2005)] and are, in addition to *pstSCAB* operons, located elsewhere in the genomes. The frequency of this co-occurrence argues against sheer coincidence, with the implication being that the *aio*-proximal *pst/pho/phn* genes may somehow be related to arsenic metabolism (Li *et al*., 2013). For this to be a reasonable initial working hypothesis, these *aio*-proximal *pstSCAB* operons should be regulated in an As^{III}-relevant fashion. This was indeed the case for *pstS*1 in strain GW4 (Supporting Information Fig. S6) and in *A. tumefaciens* strain 5A (Kang *et al*., 2012). The GW4 genome is annotated with two Pit transporters and two PstSCAB systems, and thus several possible means of As^{V} transport are available. However, the induction of *pstS1* by As^{III} in two different strains of *A. tumefaciens* (GW4 and 5A) led us to examine PstS1, presumably the primary point of contact

for solutes taken up via the PstSCAB system (Willsky and Malamy, 1980a,b; Coleman and Chisholm, 2010). Evidence gathered in the current study supports the view that PstS1 can bind As^{V} (Fig. 8), implying that PstS1 is capable of initiating As^{V} uptake, although with lower affinity than Pi.

Recent characterization of PstS proteins led to the conclusion that PstS can discriminate Pi over As^{V} by at least 500-fold, depending on the source organism (Elias *et al*., 2012). However, estimates obtained with purified PstS proteins do not necessarily reflect actual cell transport behaviour and kinetics. For example, the *Escherichia coli* PstS was estimated to discriminate against As^{V} by a factor of almost 800 (Elias *et al*., 2012). However, when As^{V} and Pi uptake were examined in a Pst-dependent *E. coli* strain at much lower As^{V} : Pi ratios, As^{V} was found to: (i) be a competitive inhibitor of Pi transport; (ii) constrain growth (i.e. exhibited toxicity); and (iii) disrupt ATP synthesis by presumably entering the cell (Willsky and Malamy, 1980a,b). As^{V} uptake became apparent for GW4 and Δ*aioA*-C at different time points (Fig. 2A and C). However, its occurrence was consistent with both strains, coinciding with As^{V} : Pi ratios in the culture fluids of approximately 40 (compare Fig. 2A and C with Fig. 3A and C). The Kd values of PstS1 (Fig. 8) are consistent with the expectation that the PstSCAB-1 system could accommodate As^{V} uptake under these conditions, which is consistent with what was actually observed (e.g. compare Fig. 2A and Fig. 3A).

As^{V} uptake (Fig. 2) led to a cellular As : Pi ratio of a remarkable 4.3:1 in early stationary phase GW4 (Table 1). In GW4, arsenic was associated with all three major cell fractions, favouring the periplasm and membrane fractions and principally as As^{V} (Fig. 4). There was no detectable arsenic in the nucleic acid extracts and thus is consistent with that observed with *Halomonas* strain GFAJ-1 (Erb *et al*., 2012; Reaves *et al*., 2012). Arsenosugars were also not detected and may be due to the lack of a detectable *arsM* in the GW4 genome. Based on the structure of known arsenosugars (Francesconi and Kuehnelt, 2002), ArsM would be required to generate methylated As^{V} prior to incorporation into carbon skeletons (Rosen *et al*., 2011).

Localization of As^{V} in the periplasm was not attempted in this study, although significant As^{V} co-extracted with proteins that may reside in the periplasm (Fig. 5). Studies with human hepatocarcinoma cells (Mizumura *et al*., 2010) suggested that interactions between proteins and As^{V} are generally non-specific, of course with the exception of As-specialized proteins such as ArsC (Martin *et al*., 2001), as well as pentavalent arsenic specifically interacting with zinc-binding sites of proteins (reviewed by Shen *et al*., 2013). As^{V} has been found to have stimulatory affects on gene expression in *Thiomonas arsenitoxydans* (Slyemi *et al*., 2013) and *Geobacillus kaustophilus* (Cuebas *et al*., 2011), although it is likely that in such experimental circumstances added As^{V} is acted upon first by low-level constitutive expression of ArsC, leading to production of As^{III} that then serves as the inducing ligand (Murphy and Saltikov, 2009).

Membranes were also a significant repository for As^{V} (Fig. 4), and thus, not surprisingly, cellular lipids were also found to contain As^{V} (Fig. 6). The influence of As^{V} on lipid composition could be seen using different assessments: (i) TLC mobility of larger polar lipids was altered (Fig. 6A); (ii) direct measurement of lipids via HPLC-HG-AFS analysis (Fig. 6B); and (iii) GC-MS-generated lipid profiles were significantly changed (Supporting Information Fig. S4). These lipids are presumably a part of the bilayer structure of the cell membrane, replacing Pi under the Pi-limiting conditions imposed in this study. Arsenolipids *per se* have been documented for decades in a variety of microbes as well as higher organisms (reviewed by Dembitsky and Levitsky, 2004) and have been suggested to replace phospholipids as a source of Pi for a Pi-starved organism (Rosen *et al*., 2011). Interestingly though, to our knowledge, all documented arsenolipids derive from the incorporation of variously methylated As^{V} species. The lack of a recognizable *arsM* homologue in GW4 (discussed above) implies that the As^{V} component of the polar lipid originated from a different biosynthesis strategy.

Lower levels of As^{III} were found in all three strains (Table 1, Fig. 4). As^{III} dominance over As^{V} in the Δ*aioA* mutant (Fig. 4) was likely simply a function of there being no/less As^{V} being available during the growth cycle (the arsenite reagent contained low levels of As^{V}). However, it is interesting that As^{III} distribution in GW4 and Δ*aioA*-C (As^{III}-oxidizing strains) favoured accumulation in the membranes as opposed to the Δ*aioA* mutant, where As^{III} was found primarily in the periplasm and cytoplasm fractions. At present, an explanation is not apparent. Based on what is currently known about As^{III} reactivity in cells (reviewed by Shen *et al*., 2013), binding to protein sulfhydryls is an important mechanism of As^{III} interaction, and studies have shown the capacity to use microbial cells as biosorbents for removing As^{III} from solution (Giri *et al*., 2013). However, neither of these generalizations should seemingly apply in this case, because based on genotype alone, the lone difference between these strains is the presence or absence of a functional As^{III} oxidase enzyme associated with the cytoplasmic membrane.

Summary

Pi levels in nature are typically quite low because of biological demand as well as the inherent chemistry of phosphorus that limits its solubility in many environments (Larsen and Court, 1961; Smil, 2000; Tiessen, 2008). This

can become an issue for As^{III}-oxidizing microorganisms, where they actively participate in elevating the As^{V} : Pi ratios in their immediate surroundings. Current views are biased towards arguments that microorganisms must be able to acquire Pi while excluding As^{V} or rid themselves of arsenic so as to avoid its toxic effects (e.g. Oremland *et al*., 2009; Wolfe-Simon *et al*., 2009; Stolz *et al*., 2010; Elias *et al*., 2012; Huertas and Michán, 2013; Slyemi *et al*., 2013). Yet, there are numerous reports documenting how various microorganisms can tolerate millimolar levels of As^{V} (Achour *et al*., 2007) and thus high tolerance is either linked to mechanisms of toxin exclusion or, alternatively, adaptations that may yield survival dividends. *A. tumefaciens* strain GW4 exhibited log phase growth and maintained viability while taking up and incorporating As^{V} into cell biomass well in excess of Pi. Clearly then, incorporation of As^{V} into select cellular material was not lethal. Therefore, we suggest that some organisms may have evolved adaptive measures whereby they actually utilize Pi substitutes in a fashion that perhaps provides a competitive edge in low-Pi environments. Pi-sparing and recycling activity has been previously documented for *Bacillus subtilis* and *Rhodobacter sphaeroides*, wherein phospholipids are replaced by sulfolipids when Pi is in short supply (Minnikin *et al*., 1972; Merad *et al*., 1989; Benning *et al*., 1995). We suggest that to ensure survival when the environmental situation demands, organisms represented by *A. tumefaciens* GW4 will readily substitute As^{V} for Pi for functions such as membrane synthesis and maintenance in order to divert Pi to critical cellular functions such as nucleic acid and ATP synthesis for which there are no known substitutes for Pi.

Experimental procedures

Strains and culture condition

Bacterial strains and plasmids used in this research are listed in Supporting Information Table S1. *A. tumefaciens* GW4 was grown in a defined minimal mannitol medium ($MMNH_4$, Somerville and Kahn, 1983) containing 54.8 mM mannitol as the primary carbon source. Cultures were incubated at 28°C in $MMNH_4$ containing 0, 0.1 or 1 mM phosphate (Pi), referred to as non-Pi, low-Pi, and normal-Pi conditions respectively. As noted, 1.0 mM $NaAsO_2$ (As^{III}) was added to the medium. *E. coli* strains were grown in Luria–Bertani (peptone, 10 g l^{-1}; yeast extract, 5 g l^{-1}; NaCl, 10 g l^{-1}) broth at 37°C. When required, 50 μg ml^{-1} of kanamycin (Kan), 50 μg ml^{-1} of gentamicin (Gen), 5 μg ml^{-1} of tetracycline (Tet) or 100 μg ml^{-1} of spectinomycin (Spe) was added.

Construction of A. tumefaciens *GW4 aioA mutant and complementation*

An in-frame deletion in *aioA* was constructed using cross-over PCR as described by Link and colleagues (1997). The primers used for the construction of the deletion are listed in Supporting Information Table S2. The final construct in plasmid pJQ200SK (pJQ-aioA) was mobilized into GW4 via conjugation with *E. coli* strain S17-1. Single cross-over mutants were identified on $MMNH_4$-Gen agar, which were then screened on $MMNH_4$ agar containing 20% sucrose, selecting for sucrose resistance resulting from resolution of the single cross-over. Gen^{Sen}, sucrose-resistant isolates were screened by PCR to identify the Δ*aioA* mutant. For complementation, the *aioBA* genes, along with the upstream RpoN-binding site, were PCR-cloned as a *Bam*HI–*Pst*I fragment (primers CaioA-F and CaioA-R, Supporting Information Table S2) into pCPP30, resulting in pCPP30-aioBA. This plasmid was transformed into *E. coli* S17-1 and conjugated into the Δ*aioA* mutant, yielding the complemented strain Δ*aioA*-C. The deletion and complementation of *aioA* were confirmed by PCR using primers PMaioA-1F/PMaioA-1R and PMaioA-2F/PMaioA-2R (Supporting Information Table S2), along with diagnostic sequencing.

Culturing, As^{III} oxidation tests and quantification of As^{III}, As^{V} and Pi

Overnight cultures of GW4, Δ*aioA* and Δ*aioA*-C (OD_{600} = 0.5-0.6) were each inoculated (200 μl) into 100 ml of $MMNH_4$ with or without 1 mmol l^{-1} of As^{III} and incubated at 28°C for 48 h with 100 r.p.m. shaking. At designated times, culture samples were taken for viable plate counts and for monitoring As^{III}/As^{V} using HPLC-HG-AFS (Beijing Titan Instruments). For the latter, culture samples were centrifuged (13 400 × *g*) to separate the cell biomass (pellet) from the culture fluids (supernatant). The supernatant was filtered (0.22 μm filter) whereas the pellets were washed three times in 20 mM Tris-HCl (pH 7.5), and then digested with 1% HNO_3 at 95°C for 2 h and adjusted to pH 6.5–7.0. As^{III}/As^{V} concentrations from the fluids and digested cell biomass were then measured by HPLC-HF-AFS (Liao *et al*., 2013). Pi concentrations in culture fluids and cell biomass were assessed by ion spectrophotometry (ISC-900, Dionex, Sunnyvale, CA, USA).

For TEM assessment of cell ultrastructure and morphology, cells were collected by centrifugation, fixed in 2% glutaraldehyde, dehydrated in a 10–100% ethanol series and embedded in Epon-Araldite. Ultra-thin sections were stained with uranyl acetate and lead citrate and final-viewed with TEM (Tecnai G^2 20 TWIN, FEI, Drive Hillsboro, OR, USA).

PstS1-binding with Pi, As^{III} and As^{V}

Purified PstS1 was incubated with different concentrations of As^{III}, As^{V} and Na_2HPO_4 at room temperature for 1 h. Tryptophan fluorescence was monitored between 340 and 360 nm (Liu *et al*., 2012) with a fluorescence spectrophotometer (PerkinElmer, Massachusetts, USA).

Cell fractionation for analysis of the As^{III}/As^{V} contents

Early stationary phase cells (32 h, Fig. 1) from low-Pi MMN medium with or without 1 mM As^{III} were collected by centrifugation (13 400 × *g*, 10 min, at 4°C) and washed three times with 20 mM Tris-HCl (pH 8.0). Cells were resuspended in

5 ml of 0.2 M Tris-HCl, pH 8.0, 0.5 M sucrose, 1 mM EDTA and 1 mM phenylmethysulfonyl fluoride. After incubating at room temperature for 30 min with 0.2 mg ml^{-1} of lysozyme, cell suspensions were centrifuged (13 400 × *g*, 10 min, 4°C), with the resulting supernatant removed and considered as the periplasm fraction. The pellet (protoplasts) was resuspended in 5 ml of cold ddH_2O and then sonicated on ice (5 min) to rupture the cells. Unbroken cells were removed by centrifugation (6700 × *g*, 3 min, 4°C), with the supernatant then subjected to ultra-centrifugation (26 400 × *g*) for 1 h to pellet the membranes. The resulting supernatant was considered cytoplasmic fraction (DeMaagd and Lugtenberg, 1986). The membrane fraction was digested with 1% HNO_3 at 95°C for 2 h, and adjusted to pH 7.0 with NaOH. The As^{III}/As^{V} contents in periplasmic, membrane and cytoplasmic fractions were analysed by HPLC-HG-AFS and arsenic species content calculated based on dry weight of the bacterial cells at 32 h.

Isolation and analysis of total protein, DNA and RNA

Early stationary phase, low-Pi cells (32 h, Fig. 1A), with or without 1.0 mM As^{III}, were collected by centrifugation (12,600 × g, 10 min, 4°C) and washed 3X with Tris-HCl (pH 7.5). Cells were resuspended in 3 ml Trizol (Invitrogen), incubated at room temperature for 10 min, then 0.6 ml chloroform added and vortexed vigorously. After phase separation, the cell preparation was centrifuged (12,600 × g for 15 min at 4°C) and the organic phase transferred into a new tube to which 0.9 ml of 100% ethanol was added and agitated. Precipitated DNA was removed by centrifugation (7260 × g for 5 min at 4°C. The total protein in the resulting supernatant was isolated by adding 4 ml isopropyl alcohol and centrifugation (12,600 × g for 10 min at 4°C), with the pellet washed 2X with 5 ml 95% ethanol containing 0.3 M guanidine hydrochloride. The final protein pellet was washed once with 5 ml acetone and then 3X with 5 ml 100% ethanol (Wang *et al*., 2007).

Total DNA from above was purified by phenol-chloroform-isoamyl alcohol (25:24:1, v/v/v) and precipitated by ethanol. After twice washed with 70% ethanol, the DNA pellet was dissolved in 100 µl sterilized H_2O (Sambrook and Russell, 2001). Total RNA was extracted used Trizol (Invitrogen) and treated with DNase I (Takara) to remove genomic DNA contamination (Wang *et al*., 2011). The As^{III}/As^{V} contents in total protein, total DNA and total RNA were quantified by HPLC-HG-AFS and calculated based on the dry weight of bacterial cells at 32 h.

Isolation and analysis of polar lipids

After cultivation for 32 h in low-Pi $MMNH_4$ medium with or without 1.0 mM As^{III}, 20 ml of culture of each strain was collected by centrifugation with 12,600 × *g* for 5 min. Polar lipids were then extracted and purified using the protocols described by Morris (1972). TLC plates were composed of silica gel G and used to separate the polar lipids by molecular weight. After pretreating the plate at 120°C for 30 min, 10 µl of polar lipid samples were loaded onto the plate and then placed into solvent chamber with 200 ml of the exhibition layer agent (128 ml of chloroform, 47.5 ml of methanol, 17.5 ml of acetone, 3.5 ml of ammonia water and 3.5 ml of ddH_2O). Plates were then removed, dried for 30 min., sprayed with 5% (w/v) phosphomolybdic acid and heated at 120°C for 10 min to visualize the lipid spots (Tornabene and Langworthy, 1979). Lipid spots were scraped from the TLC plate and then analysed for As^{III}/As^{V} contents with HPLC-HG-AFS.

Methyl esterified derivatives of the polar lipids were analysed by GC-MS (Agilent 7890A/5975C-GC/MSD, Santa Clara, CA, USA) to predict structures. Separation was achieved on an HP-5 fused silica capillary column, operated from 40°C to 250°C at 4°C min^{-1} and 8 psi He. Components were identified by comparing their retention times with established standards and their fragmentation patterns (Suen *et al*., 1987). Based on structures of known polar phospholipids and the results of GC-MS, the lipid structures were predicted.

The methods of analysis of ATP and NADH, detection of arsenosugars, SDS-PAGE analysis of total protein, and overexpression and purification of PstS are listed in the Supporting Information Appendix S1.

Acknowledgements

The present study was supported by the National Natural Science Foundation of China (31170106, 31010103903) to G.W, and in part by the U.S. National Science Foundation (MCB-0817170) to T.R.M. We would like to express our gratitude to Dr. Kevin A. Francesconi (Southern Denmark University) for providing arsenosugar standards, and Miss Jie Li for technical assistance.

References

Achour, A.R., Bauda, P., and Billard, P. (2007) Diversity of arsenite transporter genes from anrsenic-resistant soil bacteria. *Res Microbiol* **158:** 128–137.

Benning, C., Huang, Z.H., and Gage, D.A. (1995) Accumulation of a novel glycolipid and a betaine lipid in cells of *Rhodobacter sphaeroides* grown under phosphate limitation. *Arch Biochem Biophys* **317:** 103–111.

Cai, L., Liu, G., Rensing, C., and Wang, G. (2009) Genes involved in arsenic transformation and resistance associated with different levels of arsenic-contaminated soils. *BMC Microbiol* **9:** 4.

Chakraborti, D., Das, B., Rahman, M.M., Chowdhury, U.K., Biswas, B., Goswami, A.B., *et al*. (2009) Status of groundwater arsenic contamination in the state of West Bengal, India: a 20-year study report. *Mol Nutr Food Res* **53:** 542–551.

Cleiss-Arnold, J., Koechler, S., Proux, C., Fardeau, M.L., Dillies, M.A., Coppee, J.Y., *et al*. (2010) Temporal transcriptomic response during arsenic stress in *Herminiimonas arsenicoxydans*. *BMC Genomics* **11:** 709.

Coleman, M.L., and Chisholm, S.W. (2010) Ecosystem-specific selection pressures revealed through comparative population genomics. *Proc Natl Acad Sci USA* **107:** 18634–18639.

Cox, A.D., and Wilkinson, S.G. (1989) Polar lipids and fatty acids of *Pseudomonas cepacia*. *Biochim Biophys Acta* **1001:** 60–67.

Cuebas, M., Villafane, A., McBride, M., Yee, N., and Bini, E. (2011) Arsenate reduction and expression of multiple chromosomal *ars* operons in *Geobacillus kaustophilus* A1. *Microbiology* **157:** 2004–2011.

Cullen, W.R., and Reimer, K.J. (1989) Arsenic speciation in the environment. *Chem Rev* **89:** 713–764.

Dejoye, C., Vian, M.A., Lumia, G., Bouscarle, C., Charton, F., and Chemat, F. (2011) Combined extraction processes of lipid from *Chlorella vulgaris microalgae*: microwave prior to supercritical carbon dioxide extraction. *Int J Mol Sci* **12:** 9332–9341.

Dembitsky, V.M., and Levitsky, D.O. (2004) Arsenolipids. *Prog Lipid Res* **43:** 403–448.

DeMaagd, R.A., and Lugtenberg, B. (1986) Fractionation of *Rhizobium leguminosarum* cells into outer membrane, cytoplasmic membrane, periplasmic, and cytoplasmic components. *J Bacteriol* **167:** 1083–1085.

Edmonds, J.S., and Francesconi, K.A. (1987) Transformations of arsenic in the marine environment. *Experientia* **43:** 553–557.

Elias, M., Wellner, A., Goldin-Azulay, K., Chabriere, E., Vorholt, J.A., Erb, T.J., and Tawfik, D.S. (2012) The molecular basis of phosphate discrimination in arsenate-rich environments. *Nature* **491:** 134–137.

Erb, T.J., Kiefer, P., Hattendorf, B., Günther, D., and Vorholt, J.A. (2012) GFAJ-1 is an arsenate-resistant, P-dependent organism. *Science* **337:** 467–470.

Fan, H., Su, C., Wang, Y., Yao, J., Zhao, K., Wang, Y., and Wang, G. (2008) Sedimentary arsenite-oxidizing and arsenate-reducing bacteria associated with high arsenic groundwater from Shanyin, Northwestern China. *J Appl Microbiol* **105:** 529–539.

Francesconi, K.A., and Kuehnelt, D. (2002) Arsenic compounds in the environment. In *Environmental Chemistry of Arsenic*. Frankenberger, W.T., Jr (ed.). New York, USA: Dekker, pp. 51–94.

Giri, A.K., Patel, R.K., Mahapatra, S.S., and Mishra, P.C. (2013) Biosorption of arsenic (III) from aqueous solution by living cells of *Bacillus cereus*. *Environ Sci Pollut Res Int* **20:** 1281–1291.

vanden Hoven, R.N., and Santini, G.M. (2004) Arsenite oxidation by the heterotroph *Hydrogenophaga* sp. str. NT-14: the arsenite oxidase and its physiological electron acceptor. *Biochim Biophys Acta* **1856:** 148–155.

Hsieh, Y.J., and Wanner, B.L. (2010) Global regulation by the seven-component Pi signaling system. *Curr Opin Biotechnol* **13:** 198–203.

Huertas, M.J., and Michán, C. (2013) Indispensable or toxic? The phosphate versus arsenate debate. *Microb Biotechnol* **6:** 209–211.

Inskeep, W.P., McDermott, T.R., and Fendorf, S.E. (2001) Arsenic (V)/(III) cycling in soils and natural waters: chemical and microbiological processes. In *Environmental Chemistry of Arsenic*. Frankenberger, W.F., Jr, and Macy, J.M. (eds). New York, USA: Marcell Dekker, pp. 183–215.

Kang, Y.S., Heinemann, J., Bothner, B., Rensing, C., and McDermott, T.R. (2012) Integrated coregulation of bacterial arsenic and phosphorus metabolisms. *Environ Microbiol* **14:** 3097–3109.

Konova, I.V., Kochkina, G.A., and Galanina, L.A. (2005) The prevalence of cis-9-hexadecenoic acid is a specific feature of the fatty acid profile of zygomycetes from the order *Kickxellales*. *Microbiology* **74:** 86–90.

Larsen, S., and Court, M.N. (1961) Soil phosphate solubility. *Nature* **189:** 164–165.

Li, H., Li, M., Huang, Y., Rensing, C., and Wang, G. (2013) *In silico* analysis of bacterial arsenic islands reveals remarkable synteny and functional relatedness between arsenate and phosphate. *Front Microbiol* **4:** 347. doi:10.3389/fmicb.2013.00347.

Liao, S., Zhou, J., Wang, H., Chen, X., Wang, H., and Wang, G. (2013) Arsenite oxidation using biogenic manganese oxides produced by a deep-sea manganese-oxidizing bacterium, *Marinobacter* sp. MnI7–9. *Geomicrobiol J* **30:** 150–159.

Lieutaud, A., van Lis, R., Duval, S., Capowiez, L., Muller, D., Lebrun, R., *et al*. (2010) Arsenite oxidase from *Ralstonia* sp. 22: characterization of the enzyme and its interaction with soluble cytochromes. *J Biol Chem* **285:** 20433–20441.

Link, A.J., Phillips, D., and Church, G.M. (1997) Methods for generating precise deletions and insertions in the genome of wild-type *Escherichia coli*: application to open reading frame characterization. *J Bacteriol* **179:** 6228–6237.

van Lis, R., Nitschke, W., Duval, S., and Schoepp-Cothenet, B. (2013) Arsenics as bioenergetics substrates. *Biochim Biophys Acta* **1827:** 2176–2188.

Liu, G., Liu, M., Eun-Hae, K., Matty, W., Bothner, B., Lei, B., *et al*. (2012) A periplasmic arsenite-binding protein involved in regulating arsenite oxidation. *Environ Microbiol* **14:** 1624–1634.

Liu, W., Chan, A.S., Liu, H., Cochrane, S.A., and Vederas, J.C. (2011) Solid supported chemical syntheses of both components of the lantibiotic lacticin 3147. *J Am Chem Soc* **133:** 14216–14219.

Liu, Z., Carbrey, J.M., Agre, P., and Rosen, B.P. (2004) Arsenic trioxide uptake by human and rat aquaglyceroporins. *Biochem Biophys Res Commun* **316:** 1178–1185.

Liu, Z., Sanchez, M.A., Jiang, X., Boles, E., Landfear, S.M., and Rosen, B.P. (2006) Mammalian glucose permease GLUT1 facilitates transport of arsenic trioxide and methylarsonous acid. *Biochem Biophys Res Commun* **351:** 424–430.

Madsen, A.D., Goessler, W., Pedersen, S.N., and Francesconi, K.A. (2000) Characterization of an algal extract by HPLC-ICP-MS and LC-electrospray MS for use in arsenosugar speciation studies. *J Anal At Spectrom* **15:** 657–662.

Martin, P., DeMel, S., Shi, J., Gladysheva, T., Gatti, D.L., Rosen, B.P., and Edwards, B.F.P. (2001) Insights into the structure, solvation, and mechanism of ArsC arsenate reductase, a novel arsenic detoxification enzyme. *Structure* **9:** 1071–1081.

Mayilraj, S., Suresh, K., Kroppenstedt, R.M., and Saini, H.S. (2006) *Dietzia kunjamensis* sp. nov., isolated from the Indian Himalayas. *Int J Syst Evol Microbiol* **56:** 1667–1671.

Medveczky, N., and Rosenberg, H. (1970) The phosphate-binding protein of *Escherichia coli*. *Biochim Biophys Acta* **211:** 158–168.

Merad, T., Archibald, A.R., Hancock, I.C., Harwood, C.R., and Hobot, J.A. (1989) Cell wall assembly in *Bacillus subtilis*: visualization of old and new wall material by elec-

tron microscopic examination of samples stained selectively for teichoic acid and teichuronic acid. *J Gen Microbiol* **135:** 645–655.
Minnikin, D.E., Abdolrahimzadeh, H., and Baddiley, J. (1972) Variation of polar lipid composition of *Bacillus subtilis* (Marburg) with different growth conditions. *FEBS Lett* **27:** 16–18.
Mizumura, A., Watanabe, T., Kobayashi, Y., and Hirano, S. (2010) Identification of arsenite and arsenic diglutathione-binding proteins in human hepatocarcinoma cells. *Toxicol Appl Pharmacol* **242:** 119–125.
Morita, M., and Shibata, Y. (1988) Isolation and identification of arseno-lipid from a brown alga, *Undariapinnatifida* (Wakame). *Chemosphere* **17:** 1147–1152.
Morris, K. (1972) Techniques of lipidology: isolation, analysis, and identification of lipids. In *Laboratory Techniques in Biochemistry and Molecular Biology*. Burden, R.H., and van Kippenburg, P.H. (eds). New York, USA: Elsevier, pp. 232–254.
Murphy, J.N., and Saltikov, C.W. (2009) The ArsR repressor mediates arsenite-dependent regulation of arsenate respiration and detoxification operons of *Shewanella* sp. Strain ANA-3. *J Bacteriol* **191:** 6722–6731.
Müller, R.H., Loffhagen, N., and Babel, W. (1996) Rapid extraction of (di)nucleotides from bacterial cells and determination by ion-pair reversed-phase HPLC. *J Microbiol Methods* **25:** 29–35.
Oremland, R.S., and Stolz, J.F. (2005) Arsenic, microbes and contaminated aquifers. *Trends Microbiol* **13:** 45–49.
Oremland, R.S., Saltikov, C.W., Wolfe-Simon, F., and Stolz, J.F. (2009) Arsenic in the evolution of earth and extraterrestrial ecosystems. *Geomicrobiol J* **26:** 522–536.
Páez-Espino, D., Tamames, J., de Lorenzo, V., and Cánovas, D. (2009) Microbial responses to environmental arsenic. *Biometals* **22:** 117–130.
Rakotomanga, M., Saint-Pierre-Chazalet, M., and Loiseau, P.M. (2005) Alteration of fatty acid and sterol metabolism in miltefosine-resistant *Leishmania donovani* promastigotes and consequences for drug-membrane interactions. *Antimicrob Agents Chemother* **49:** 2677–2686.
Reaves, M.L., Sinha, S., Rabinowitz, J.D., Kruglyak, L., and Redfield, R.J. (2012) Absence of detectable arsenate in DNA from arsenate-grown GFAJ-1 cells. *Science* **337:** 470–473.
Rodríguez-Lado, L., Sun, G., Berg, M., Zhang, Q., Xue, H., Zheng, Q., and Johnson, C.A. (2013) Groundwater arsenic contamination throughout China. *Science* **341:** 866–868.
Rosen, B.P. (2002) Biochemistry of arsenic detoxification. *FEBS Lett* **529:** 86–92.
Rosen, B.P., Ajees, A.A., and McDermott, T.R. (2011) Life and death with arsenic. *Bioessays* **33:** 350–357.
Sambrook, J., and Russell, D.W. (2001) *Molecular Cloning: A Laboratory Manual*, Vol. 1–3. Cold Spring Harbor, NY, USA: Cold Spring Harbor Laboratory Press.
Santini, J.M., Kappler, U., Ward, S.A., Honeychurch, M.J., and Bernhardt, P.V. (2007) The NT-26 *cytochrome* c_{552} and its role in arsenite oxidation. *Biochim Biophys Acta* **1767:** 189–196.
Shen, S., Li, X.F., Cullen, W.R., Weinfeld, M., and Le, X.C. (2013) Arsenic binding to proteins. *Chem Rev* **113:** 7769–7792.
Silver, S., and Phung, L.T. (2005) Genes and enzymes involved in bacterial oxidation and reduction of inorganic arsenic. *Appl Environ Microbiol* **71:** 599–608.
Slyemi, D., and Bonnefoy, V. (2012) How prokaryotes deal with arsenic. *Environ Microbiol Rep* **4:** 571–586.
Slyemi, D., Moinier, D., Talla, E., and Bonnefoy, V. (2013) Organization and regulation of the arsenite oxidase operon of the moderately acidophilic and facultative chemoautotrophic *Thiomonas arsenitoxydans*. *Extremophiles* **17:** 911–920.
Smil, V. (2000) Phosphorus in the environment: natural flow and human interferences. *Annu Rev Energy Environ* **25:** 53–88.
Somerville, J.E., and Kahn, M.L. (1983) Cloning of the glutamine synthetase I gene from *Rhizobium meliloti*. *J Bacteriol* **156:** 168–176.
Stolz, J.F., Basu, P., Santini, J.M., and Oremland, R.S. (2006) Arsenic and selenium in microbial metabolism. *Annu Rev Microbiol* **60:** 107–130.
Stolz, J.F., Basu, P., and Oremland, R.S. (2010) Microbial arsenic metabolism: new twists on an old poison. *Microbe* **5:** 53–59.
Suen, Y., Hubbard, J.S., Holzer, G., and Tornabene, T.G. (1987) Total lipid production of the green alga *Nannochloropsis* sp. QII under different nitrogen regimes. *J Phycol* **23:** 289–296.
Tiessen, H. (2008) Phosphorus in the global environment. In *The Ecophysiology of Plant-Phosphorus Interactions*. White, P.J., and Hammond, J.P. (eds). Dordrecht, Netherlands: Springer, pp. 1–7.
Tornabene, T., and Langworthy, T. (1979) Diphytanyl and dibiphytanyl glycerol ether lipids of methanogenic *Archaebacteria*. *Science* **203:** 51–53.
Wang, Q., Xiong, D., Zhao, P., Yu, X., Tu, B., and Wang, G. (2011) Effect of applying an arsenic-resistant and plant growth-promoting rhizobacterium to enhance soil arsenic phytoremediation by *Populus deltoides* LH05–17. *J Appl Microbiol* **111:** 1065–1074.
Wang, X., Li, X., Deng, X., Han, H., Shi, W., and Li, Y. (2007) A protein extraction method compatible with proteomic analysis for the euhalophyte *Salicorniaeuropaea*. *Electrophoresis* **28:** 3976–3987.
Willsky, G.R., and Malamy, M.H. (1980a) Characterization of two genetically separable inorganic P transport systems in *Escherichia coli*. *J Bacteriol* **144:** 356–365.
Willsky, G.R., and Malamy, M.H. (1980b) Effect of arsenate on inorganic phosphate transport in *Escherichia coli*. *J Bacteriol* **144:** 366–374.
Wolfe-Simon, F., Davies, P.C.W., and Anbar, A.D. (2009) Did nature also choose arsenic? *Int J Astrobiol* **8:** 69–74.

Supporting information

Additional Supporting Information may be found in the online version of this article at the publisher's web-site:

Fig. S1. The physical map of the *pst-pho-aio* gene islands in *A. tumefaciens* strains GW4 and 5A, and the primer locations of PMaioA-1F, PMaioA-1R, PMaioA-2F and PMaioA-2R used in cross-over PCRs to generate the Δ*aioA* mutant (Supporting Information Table S1). The *pstS1* coding region is high-

lighted with cross-hatch. The nucleotide accession number of the genes in the *pst-pho-aio* gene islands in strain GW4 are shown in Supporting Information Table S3.

Fig. S2. Diagnostic PCR confirming the deletion of *aioA* to create mutant strain Δ*aioA* and complementation to create Δ*aioA*-C.

A. PCR amplicons using primers PMaioA-1F and PMaioA-1R (see Supporting Information Fig. S1).

B. PCR amplicons using primers PMaioA-2F and PMaioA-2R (Supporting Information Fig. S1).

For both panels: Lane 1, strain GW4, lane 2, *aioA* gene knock-out strain Δ*aioA*, and lane 3, the complemented strain Δ*aioA*–C. M, the molecular weight marker (DL 2000 plus). Amplicon identities were confirmed by DNA sequencing.

Fig. S3. Cellular energy metabolites as a function of capacity to oxidize As^{III}, medium Pi content (L, low; N, normal), and presence or absence of 1.0 mM As^{III}. Cellular concentrations in *A. tumefaciens* strains GW4, Δ*aioA* and Δ*aioA*-C of:

A. NADH.

B. ATP.

Metabolites were extracted from log phase cultures. Data are shown as the mean of three replicates, with the error bars (where visible) illustrating one standard deviation.

Fig. S4. Relative polar lipid composition in strains GW4, Δ*aioA* and Δ*aioA*-C cultured with or without As^{III}. Red vertical arrow in each panel identifies the standard eluting at 21.6 min, while black arrows in A and C panels identify the possible arsenolipids eluting at 23.7 min.

Fig. S5. Altered cell morphology associated with high concentrations of As^{V} in the cell environment. Cells of *A. tumefaciens* wild-type strain GW4 and the Δ*aioA* mutant were cultured without (–) or with (+) 1.0 mM As^{III} in low-Pi medium, and then prepared for transmission electron microscopy viewing. Lower panels are sub-sample enlargement images derived from the panel directly above it. OM, outer membrane; CM, cytoplasmic membrane. Red scale bars for all panels and both magnifications represent 500 mm. Distinguishing the OM and CM for the Δ*aioA* mutant was problematic.

Fig. S6. Identification and purification of *A. tumefaciens* GW4 PstS.

A. The SDS-PAGE of partial proteins isolated from the bacterial cells cultured in $MMNH_4$ with 100 uM Pi for 32 h. M, molecular weight standards; Lane 1, + As^{III} cells; Lane 2, –As^{III} cells. Arrow indicates the position of PstS identified with mass spectrometry.

B. Over-expressed PstS without the signal peptide and with a His_6 tag in *E. coli* BL21. Lane 1 was the total protein in strain BL21 (pET-pstS); Lane 2, purified PstS.

Table S1. The strains and plasmids used in this research.

Table S2. Primers used in this research.

Table S3. The GenBank accession numbers of the genes involved in the *pst-pho-aio* gene islands of strain GW4.

Appendix S1. Supporting Methods.